

Decoupling of global brain activity and cerebrospinal fluid flow in Parkinson's cognitive decline

Short running title: fMRI glymphatic and cognitive deficit

Feng Han¹, Gregory L. Brown^{2,3}, Yalin Zhu¹, Aaron E. Belkin-Rosen¹, Mechelle M. Lewis^{3,4},
Guangwei Du³, Yameng Gu¹, Paul J. Eslinger^{3,5}, Richard B. Mailman^{3,4}, Xuemei Huang^{3,4,5,6,7,8}
*, Xiao Liu^{1,8} *.

Affiliations:

¹Department of Biomedical Engineering, The Pennsylvania State University, PA, USA;

²Department of Engineering Science and Mechanics, The Pennsylvania State University, PA, USA;

³Department of Neurology, Pennsylvania State University Milton S. Hershey Medical Center, Hershey, PA, USA;

⁴Department of Pharmacology, Pennsylvania State University Milton S. Hershey Medical Center, Hershey, PA, USA;

⁵Department of Radiology, Pennsylvania State University Milton S. Hershey Medical Center, Hershey, PA, USA;

⁶Department of Neurosurgery, Pennsylvania State University Milton S. Hershey Medical Center, Hershey, PA, USA;

⁷Department of Kinesiology, Pennsylvania State University Milton S. Hershey Medical Center, Hershey, PA, USA;

⁸Institute for Computational and Data Sciences, The Pennsylvania State University, PA, USA;

*Correspondence to:

Dr. Liu (xxl213@engr.psu.edu) or Dr. Huang (xuemei@psu.edu)

Abstract

Background: Deposition and spreading of misfolded proteins (α -synuclein and tau) have been linked to Parkinson's cognitive dysfunction. The glymphatic system may play an important role in the clearance of these toxic proteins via cerebrospinal fluid (CSF) flow through perivascular and interstitial spaces. Recent studies discovered that sleep-dependent global brain activity is coupled to CSF flow that may reflect glymphatic function.

Objective: To determine if the decoupling of brain activity-CSF flow is linked to Parkinson's cognitive dysfunction.

Methods: Functional and structural MRI data, clinical motor (Unified Parkinson's Disease Rating Scale), and cognitive (Montreal Cognitive Assessment, MoCA) scores were collected from 60 Parkinson's and 58 control subjects. Parkinson's patients were subgrouped into those with ($\text{MoCA} < 26$; $N = 29$) and without ($\text{MoCA} \geq 26$; $N = 31$) mild cognitive impairment (MCI). The coupling strength between the resting-state global blood-oxygen-level-dependent signal (gBOLD) and associated CSF flow was quantified, compared among groups, and associated with clinical and structural measurements.

Results: gBOLD-CSF coupling decreased significantly ($p < 0.006$) in Parkinson's patients showing MCI, compared to those without MCI and controls. Reduced gBOLD-CSF coupling was associated with decreased MoCA scores that was present in Parkinson's patients ($p = 0.005$) but not in controls ($p = 0.65$). Weaker gBOLD-CSF coupling in Parkinson's patients also was associated with a thinner right entorhinal cortex (Spearman's correlation = -0.36 ; $p = 0.012$), an early structural change often seen in Alzheimer's.

Conclusions: The decoupling between global brain activity and associated CSF flow is related to Parkinson's cognitive impairment.

Keywords: cerebrospinal fluid flow (CSF); cognitive impairment; glymphatic system; global resting-state fMRI signal; Parkinson's disease.

Parkinson's disease is characterized clinically by motor dysfunction¹ and pathologically by both α -synuclein-positive Lewy bodies/neurites and dopamine neuron loss in the substantia nigra pars compacta of the basal ganglia.² Recent literature also highlights non-motor features of the disease, with cognitive decline being one of the most debilitating symptoms. Indeed, >75% of Parkinson's patients who survive for more than 10 years ultimately develop dementia.³ The exact mechanisms contributing to cognitive decline in Parkinson's disease (**PD**) are unknown and probably multifactorial. Many pathological processes have been proposed. The aggregation and spreading of α -synuclein to extra-nigral subcortical and cortical structures^{4,5} is one prominent hypothesis. Superimposed Alzheimer's disease (AD) pathology⁶⁻⁹ could be another cause, since moderate to severe Alzheimer's-co-pathology (e.g., amyloid- β and tau) has been found in 51% of PD patients, and is associated with faster time to dementia than Parkinson's pathology alone.¹⁰

Increasing evidence suggests an important role of a newly discovered "glymphatic system" in clearing toxic proteins from the brain;¹¹ these include α -synuclein,^{12,13} amyloid- β ,¹⁴ and tau.¹⁵ In this clearance pathway, cerebrospinal fluid (**CSF**) flows into the interstitial space through the periaxonal space, facilitated by astroglial aquaporin-4 water channels. The bulk CSF flow then drives interstitial fluid (**ISF**) flux and interstitial solutes/proteins into the perivenous space around deep-draining veins where they eventually are transported into the lymphatic system.^{11,14,16} Intriguingly, the glymphatic system functions mainly during sleep, but much less engaged during the awake state.¹¹ This leads to the hypothesis that this "waste clearance" function is one universal mechanism contributing to the need for sleep in all species. This may also explain a diurnal rhythm of amyloid- β , tau, and α -synuclein.^{15,17,18}

Despite its potential role in cognitive dysfunction and dementias, the study of the glymphatic system in humans has been challenging, largely due to a lack of tools that can assess glymphatic function directly and non-invasively. Two-photon microscopy and fluorescence imaging are used commonly in animal studies of the glymphatic system, but cannot yet be applied to human subjects.^{19,20} Contrast-enhanced MRI has been employed to track whole-brain CSF flow, including in human subjects,^{21,22} but broad application is limited by the need for intrathecal contrast agents and the long-duration experiments. Diffusion and structural MRI have been proposed to probe glymphatic function through surrogate markers such as perivascular space,^{22–24} however, they do not directly reflect dynamic aspects of the glymphatic system.

The pioneering study of Kiviniemi et al.²⁵ suggested that low-frequency (<0.1 Hz) resting-state fMRI (rsfMRI) blood-oxygen-level-dependent (**BOLD**) signals are linked to CSF dynamics and, thus, glymphatic function. Additional evidence supports the link between global brain activity (measured by BOLD) and glymphatic function. First, the global BOLD (**gBOLD**) signal, like glymphatic function, is highly sensitive to brain vigilance state, and also has large-amplitude fluctuations during drowsiness or sleep.^{26–28} Second, the gBOLD signal is accompanied by profound low-frequency (<0.1 Hz) physiological changes including in cardiac pulsation,^{29–31} respiration,^{32–34} and arterial signals.³⁵ These latter physiological functions have been hypothesized to drive glymphatic CSF flow.^{36–40} Third, the large gBOLD signal during sleep was reported to couple to strong CSF movement⁴¹ that is an essential component of the glymphatic system. Collectively, the resting-state global activity and associated physiological modulations are hypothesized to represent highly coordinated neural and physiological processes closely linked to glymphatic clearance. Thus, the gBOLD-CSF coupling may serve as a marker for gauging glymphatic function.

There is limited research on the role of the glymphatic system in PD or even in PD animal models, in part because α -synuclein conformational changes and accumulation were believed to occur within neurons or at presynaptic terminals.⁴² Recent evidence, however, indicates that α -synuclein is secreted into brain extracellular spaces,⁴³ suggesting a potential role of glymphatic clearance in PD. Similar to amyloid- β and tau, α -synuclein in both ISF and CSF increased in response to sleep deprivation.¹⁵ In addition, tau protein, which can be cleaned by glymphatic system,⁴⁴ plays an important role in the development of PD and PD dementia.^{7,45,46} Thus, we hypothesized that coupling between the global brain signal and CSF flow is related to glymphatic function and thus cognitive impairment in Parkinson's patients.

Methods

Study design and participants

Sixty PD subjects and 58 controls for whom we had rsfMRI data and Montreal Cognitive Assessment (MoCA) scores were included. The PD subjects were recruited from a tertiary movement disorders clinic and controls from the spouse population of the clinic or via IRB-approved recruitment materials posted in the local community. PD diagnosis was confirmed by a movement disorder specialist according to the UK Brain Bank criteria.⁴⁷ All subjects were free of major/unstable medical issues such as liver, kidney, or thyroid abnormality, and deficiency of vitamin B₁₂, or any cerebrovascular disease or neurological condition (other than PD). Disease duration was obtained from subject history, with onset defined as the first diagnosis by a medical professional.

Ethics approval

The full protocol of this study was approved by the Institutional Review Board of Human Subjects Protection Office at the Penn State Milton S. Hershey Medical Center College of Medicine. All subjects provided written informed consent. The study was conducted in accordance with the principles of the Declaration of Helsinki.

Clinical assessments

The Movement Disorder Society (MDS)-UPDRS sub-scores (UPDRS-I, UPDRS-II, and UPDRS-III) were obtained. UPDRS-I evaluates non-motor aspects of daily living, UPDRS-II assesses motor aspects of daily living reported by the subjects, and UPDRS-III evaluates motor symptoms assessed by a trained examiner.^{48,49} Levodopa-equivalent daily dosage (LEDD) was calculated for Parkinson's subjects according to published criteria.⁵⁰ Cognition was assessed using the Montreal Cognitive Assessment (MoCA)⁵¹ and depression by the Hamilton Depression Rating Scale (HAM-D).⁵² Following procedures reported in previous studies,^{51,53} Parkinson's patients were subgrouped into those with (MoCA < 26) and without (MoCA ≥ 26) mild cognitive impairment (MCI).

Image acquisition and preprocessing

All MRI data were obtained on a 3.0 Tesla MR scanner (Trio, Siemens Magnetom, Erlangen, Germany, with an 8-channel phased-array head coil). To avoid systematic bias, Parkinson's and control subjects were scanned in an intermixed fashion throughout the study. Each rsfMRI acquisition began with a T1-weighted MPRAGE structural MRI sequence (repetition time/echo time (TR/TE) = 1540/2.3 msec, field of view = 256 mm × 256 mm, matrix = 256 × 256, slice thickness = 1 mm, slice number = 176) that was used for anatomical segmentation and template normalization. In each rsfMRI session, we acquired 240 fMRI

volumes using a 3D echo-planar image (EPI) sequence (flip angle = 90° , spatial resolution = $3 \times 3 \times 4 \text{ mm}^3$, slice thickness = 3.0 mm) with TR/TE = 2000/30 msec.

RsfMRI data were preprocessed with a rsfMRI preprocessing pipeline adapted from the 1000 Functional Connectomes Project (version 1.1-beta).⁵⁴ Specifically, we performed motion correction, skull/edge stripping, spatial smoothing (full width at maximum (FWHM) = 4mm), bandpass filtering (0.01-0.1 Hz), and linear and quadratic detrending. In addition, the first five rsfMRI volumes were discarded to avoid unsteady state of magnetization and potential edge effect of temporal filtering. These procedures generated the preprocessed rsfMRI at individual space, from which the gBOLD and CSF signals were extracted. Similar to approach of Fultz et al.,⁴¹ we skipped the nuisance regression of gBOLD and CSF signal since these variables were the focus of the current study. Head motion also may affect the gBOLD signal,³⁴ and we thus tested its effects separately by regarding the head motion as a confounding factor as described below. To derive the fMRI-based drowsiness index³⁴ (see below), we further registered spatially the rsfMRI images to the standard MNI-152 space⁵⁵ (spatial resolution: $3 \times 3 \times 3 \text{ mm}$) and (temporally) standardized signals of each voxel to Z scores.

Because there is a great deal of research related to early-stage Alzheimer's disease,⁵⁶⁻⁵⁹ we quantified entorhinal cortex (**ERC**) thickness and hippocampal volume from both hemispheres using Free-Surfer (version 5.1.0) from T1-weighted images.⁶⁰ These two markers for early-stage or preclinical Alzheimer's were selected because Parkinson's subjects in our cohort have relatively high MoCA scores (mean MoCA was 24.8) compared to that for diagnosing Alzheimer's (MoCA < 18).⁶¹ The process included motion correction, tissue classification, brain extraction, registration, and segmentation of gray matter volumetric structures, such as the ERC and hippocampus. To control for inter-subject variability of brain

size, we normalized the ERC thickness and hippocampal volume with estimated total brain tissue volume.⁶²

Coupling between gBOLD signal and CSF flow

The gBOLD signal was extracted from the gray matter regions.^{33,63} It was defined based on the Harvard-Oxford cortical and subcortical structural atlases.⁶⁴ To avoid spatial blurring from the registration process, this gray-matter mask was transformed from the MNI-152 space back to the original space of each subject based on the same rationale used in a previous study.⁴¹ The fMRI signal temporally was Z-normalized and then spatially averaged across all gray matter voxels. The resulting gBOLD signal reflects the amplitude and synchronization level of global brain activity. The CSF signal was extracted from the bottom slice of the fMRI acquisition near the bottom of the cerebellum and normalized by the temporal mean to percentage change. This bottom slice is expected to have maximal sensitivity to inflow effects:⁶⁵ CSF inflow from outside the fMRI acquisition volume, which has not experienced repeated radiofrequency pulses, would increase the fMRI signal.⁴¹ The mask of CSF regions was obtained manually based on increased image intensity compared to surrounding brain regions in T2*-weighted fMRI and confirmed with T1-weighted MRI images.

Following procedures from Fultz et al.,⁴¹ the cross-correlation function first was calculated between the gBOLD and CSF signals to quantify their cross-correlations at different time lags (the gBOLD was regarded as the reference). The gBOLD-CSF cross-correlation at the time lag of +4 seconds, where the negative peak was found, was employed to quantify the gBOLD-CSF coupling for each subject. We also calculated the cross-correlation function between the negative firstorder derivative of the gBOLD signal and the CSF signal to compare with findings from Fultz et al.⁴¹ We used a permutation method to test the statistical significance

for the above gBOLD-CSF cross-correlations. The gBOLD and CSF signals from different subjects were matched randomly and their cross-correlation functions were computed and averaged. This procedure was repeated 10,000 times to build a null distribution for the mean gBOLD-CSF cross-correlation function, which then was used for statistical inference.

Comparison of gBOLD-CSF coupling and association with clinical metrics

A linear regression was first conducted between the gBOLD-CSF coupling and age, and the two-sample t test then was then used to compare the gBOLD-CSF coupling between males and females. After these two initial analyses, the age- and gender-adjusted gBOLD-CSF coupling was used for all subsequent analyses described below.

We compared gBOLD-CSF coupling among control, PD-MCI (MoCA < 26), and PD-non-MCI (MoCA \geq 26) subjects using the two-sample t-test. We then used Spearman's correlations to quantify associations between gBOLD-CSF coupling and various clinical measures, including MoCA scores, MDS-UPDRS scores, ERC thickness, and hippocampal volumes. These correlational analyses were conducted within the control (if applicable) and PD groups, as well as the entire group of subjects.

We further evaluated the potential effects of multiple factors, including high-leverage data point, disease duration, head motion, and arousal state, on the association between the gBOLD-CSF coupling and MoCA score. We re-ran the correlation between the two after excluding two high-leverage data points with MoCA less than 15, as well as controlling for disease duration. We estimated head motion and drowsiness/sleepiness level of subjects and then re-tested the association between gBOLD-CSF coupling and MoCA controlling for these factors. For head motion, we quantified framewise displacement (FD), is defined as the sum of the

absolute values of six translational and rotational motion parameters.⁶⁶ These values then were averaged within the same session to quantify individual subject head motion.³⁴ For the arousal state, we adapted an fMRI-based drowsiness index.^{34,67} Briefly, we computed the spatial correlation between each rsfMRI volume and a pre-defined drowsiness template derived previously²⁸ and then took the envelope amplitude of this spatial correlation (i.e., similarity) as an estimation of instantaneous brain arousal level. This drowsiness index then was averaged within each session to represent the overall drowsiness level of each subject and included in the correlation analysis.

Statistical analysis

In summary, the two-sample t-test was used for group comparisons of continuous demographic and clinical measures, whereas the Fisher exact test was utilized for categorical metrics.⁶⁸ The permutation test was used to assess the statistical significance of the gBOLD-CSF correlations tested. Spearman's correlation was used to quantify inter-subject associations between the gBOLD-CSF coupling and various clinical measures in order to account for potential non-normality of these variables. P-values < 0.05 were considered statistically significant. We also corrected multiple comparisons using the Bonferroni method.⁶⁹

Results

Participant characteristics

Demographic and clinical data are presented in **Table 1**. PD participants on average were ca. 3-years older than controls ($p = 0.027$). The two groups had similar numbers of males and females ($p = 0.58$). PD participants had an average disease duration of 6.6 ± 5.7 years, and

significantly higher HAM-D ($p = 4.3 \times 10^{-5}$) and lower MoCA scores ($p = 0.009$) than controls. There were approximately equal numbers of normal cognition PD patients (MoCA ≥ 26 , $N = 31$) and those with MCI (MoCA < 26 , $N = 29$).

gBOLD signal is coupled to CSF signal changes

We first examined whether the gBOLD signal is coupled to strong CSF signal changes in this Parkinson's dataset. As shown in a representative control, changes in the gBOLD signal are associated with large CSF signal changes (**Fig. 1B**, black and gray arrows). The mean gBOLD-CSF cross-correlation function was characterized by a positive peak ($r = 0.28$; $p < 0.0001$; permutation test, $N = 10,000$) around the -4 -sec lag (i.e., correlation with shifting CSF ahead of time by ca. 4 sec), whereas there was a negative peak ($r = -0.28$; $p < 0.0001$) at the lag of $+4$ sec (**Fig. 1C**, left panel). The cross-correlation function between the CSF signal and the negative first-order derivative of the gBOLD signal displayed a large positive peak at the zero time-lag ($r = 0.37$; $p < 0.0001$). Overall, both cross-correlation functions (**Fig. 1C**) showed patterns consistent with the data of Fultz et al.,⁴¹ confirming a systematic coupling between the global brain signal and CSF flow.

Comparison of gBOLD-CSF coupling among groups

We tested whether the gBOLD-CSF coupling was affected by age or gender. A significant correlation was found between age and gBOLD-CSF coupling (**Fig. 2A**; $\rho = 0.32$, $p < 0.001$), with increased age associated with weaker (less negative) gBOLD-CSF coupling. No significant difference ($p = 0.44$) in gBOLD-CSF coupling was found between males and females.

For scientific rigor, we controlled for the age and gender effects on gBOLD-CSF coupling for all subsequent analyses.

The gBOLD-CSF coupling metric then was compared among groups. PD-MCI subjects showed significantly weaker gBOLD-CSF coupling (**Fig. 2B**) than controls ($p = 0.003$) and PD-non-MCI ($p = 0.006$) subjects. gBOLD-CSF coupling strength, however, was not different between control and PD-non-MCI subjects ($p = 0.96$).

Association between gBOLD-CSF coupling and cognitive and PD measures

The gBOLD-CSF coupling then was correlated with various clinical and structural measurements. Consistent with comparisons across disease groups, weaker (less negative) gBOLD-CSF coupling was correlated significantly with lower MoCA scores across all PD subjects ($\rho = -0.36$, $p = 0.005$, $p_{\text{Bonferroni}} = 0.01$, **Fig. 2D**) but not across the controls ($\rho = -0.06$, $p = 0.65$, **Fig. 2C**). The Parkinson's-specific gBOLD-CSF coupling/MoCA associations remained significant ($\rho = -0.31$, $p = 0.017$, $p_{\text{Bonferroni}} = 0.034$, **Fig. 2E**) when excluding two subjects with very low MoCA scores. The association is also significant ($p < 0.05$) across the entire group of subjects (**Suppl. Fig. 1**), or after controlling for disease duration (**Suppl. Fig. 2**), head motion (**Suppl. Fig. 3**), and drowsiness score (**Suppl. Fig. 4**). As seen **Suppl. Fig. 5**, there was no significant correlation found between the gBOLD-CSF coupling and any of the MDS-UPDRS motor (UPDRS-II, $p = 0.80$, UPDRS-III, $p = 0.27$); or non-motor subscores UPDRS-I, $p = 0.49$).

Association of BOLD-CSF coupling strength with structural changes in Parkinson's

Weaker (less negative) gBOLD-CSF coupling was associated significantly with a thinner right ERC region ($\rho = -0.36$, $p = 0.012$, $p_{\text{Bonferroni}} = 0.024$, **Fig. 3A**), whereas only a trend was found for the left ERC thickness ($\rho = -0.19$, $p = 0.19$, $p_{\text{Bonferroni}} = 0.38$, **Fig. 3B**). Weaker

gBOLD-CSF coupling was not associated with lower hippocampal volume bilaterally ($p > 0.05$; **Suppl. Figs. 6A-B**). There was no correlation between gBOLD-CSF coupling and ERC thickness or hippocampal volume in the control group ($p > 0.05$; see **Suppl. Fig. 7**).

Discussion

The current study demonstrated a strong coupling between global brain activity and CSF flow using rsfMRI data obtained both from Parkinson's and control subjects, consistent with the idea that gBOLD-CSF coupling is related to glymphatic function. The strength of this gBOLD-CSF coupling was significantly lower in those Parkinson's patients with cognitive impairment compared to either controls or Parkinson's patients without cognitive dysfunction. Moreover, the gBOLD-CSF coupling strength was correlated with cognitive scores, but only in Parkinson's patients and not controls, suggesting it is linked to Parkinson's-related processes. No correlation was found between gBOLD-CSF coupling and UPDRS motor or non-motor scores, suggesting it is related specifically to a cognitive component of Parkinson's. The reduced gBOLD-CSF coupling also was associated with a thinner ERC that has been observed in early-stage Alzheimer's, suggesting a possible contribution from Alzheimer's-like pathology in PD-MCI. These findings suggest that gBOLD-CSF coupling is a potential noninvasive marker for the glymphatic function that may be related to dementia pathology.

gBOLD-CSF coupling may be related to the sleep-dependent glymphatic system

Resting-state gBOLD-CSF coupling likely results from highly coordinated neural and physiological processes that are linked closely to glymphatic clearance. This potential relationship is supported by at least three lines of evidence. First, the resting-state gBOLD signal shows a similar sleep dependency as glymphatic function, and is strongly promoted by

drowsiness and sleep.^{26,27,70–72} Sleep deprivation⁷¹ and hypnotic drugs (e.g., midazolam),⁷³ significantly enhance the gBOLD signal, whereas caffeine has the opposite effect.⁷² It became clear recently that the strong gBOLD signal fluctuation reflects transient arousal modulations of 10-20 sec.²⁸ Second, this gBOLD signal is accompanied by slow (<0.1 Hz), but strong physiological modulations of cardiac,^{29–31} respiratory,^{33,34} and arterial³⁵ signals. These physiological modulations have been hypothesized to be the main drivers of glymphatic CSF flow.^{36–40} It is likely that they are mediated through the autonomic system via transient arousal variations underlying the gBOLD signal.²⁹ In at least one mouse model (for cerebral amyloid angiopathy), the low-frequency modulations in vessel tone has been linked to amyloid- β clearance.⁷⁴ Thus, the gBOLD signal and associated physiological modulations should provide sleep-dependent dynamics for CSF flow that are essential for the glymphatic system. Indeed, we found that strong CSF movements coupled to the large gBOLD signal,⁴¹ adding a new piece of evidence for their relevance to the glymphatic system. This coupling relationship was confirmed and extended in the present study of Parkinson's patients. Overall, this potential link to the glymphatic system could be the primary explanation for the association we found between gBOLD-CSF coupling and cognitive dysfunction in Parkinson's.

gBOLD-CSF coupling may be a new functional metric for cognitive decline

The introduction summarized evidence for the glymphatic system being involved in clearance of toxic misfolded proteins such as α -synuclein, amyloid- β and tau, thereby possibly contribute to the cognitive decline in PD patients. The initial test of this hypothesis in the current study indicated that gBOLD-CSF coupling was decreased significantly only in Parkinson's patients with cognitive decline. It is also correlated with cognitive MoCA scores, but not with motor and other non-motor symptoms measured by MDS-UPDRS scores. Together, the data

provide the first evidence that gBOLD-CSF coupling may serve as a new, non-invasive, functional metric for quantifying cognitive decline, and warrants future studies of its relationship to the ultimate development of dementia in PD.

gBOLD-CSF coupling may reflect aspects of Alzheimer's pathology

The present study showed that weaker gBOLD-CSF coupling was associated with a thinner right ERC, although correlations with left ERC thickness or bilateral hippocampal volumes did not reach statistical significance. Right ERC thinning and early loss of ERC symmetry has been suggested a marker for preclinical Alzheimer's.^{75,76} A more pronounced loss in right ERC thickness also is seen with aging.⁷⁷ In Alzheimer's patients, gray matter loss in the right ERC has been shown to occur earlier and be larger than in other brain regions.⁷⁵ In fact, the ERC is known to be the earliest affected brain region in both Alzheimer's and Parkinson's.^{78–80} Thus, decreased gBOLD-CSF coupling may be an indicator of early cognitive decrements, and its correlation with cognitive impairment in PD-MCI may be attributed partly to structural changes similar to those in in early Alzheimer's.

Limitations and future directions

The present study linked the gBOLD-CSF coupling to cognitive dysfunction in PD, but one clear limitation of the present study was that it did not directly link the gBOLD-CSF coupling to accumulation of toxic chemical species (proteins or small molecules). This provides a fertile area for mechanistic understanding of the association of gBOLD-CSF coupling with cognitive impairment. Future studies should also explore other imaging markers that result from the same low-frequency global brain activity and physiological modulations, and relate them to cognitive decline and dementias. Related experiments could include quantification of α -

synuclein and tau (either with PET imaging or CSF measurements), metabolomic studies of CSF, and longitudinal studies of how gBOLD-CSF coupling relates to the prognosis and progression of Parkinson's disease dementia. Finally, despite the recent evidence, the relationship between gBOLD-CSF coupling and the glymphatic system remains hypothetical, and direct evidence using both murine and non-human primate models will be very important.

Acknowledgements

We thank Jiaxuan Diao for preparing some figures and reviewing the manuscript.

Author Roles

Research project: A. Conception, B. Organization, C. Execution;

Statistical Analysis: A. Design, B. Execution, C. Review and Critique;

Manuscript Preparation: A. Writing of the first draft, B. Review and Critique;

FH: 1A, 1B, 1C, 2B, 2C, 3A;

GLB: 1C, 2C, 3A, 3B;

YZ: 1C, 2B;

AEBR: 1C, 2B;

MML: 2C, 3A, 3B;

GD: 2C, 3B;

YG: 1C, 2C;

PJR: 3B;

359 **RBM:** 2C, 3B;
 360 **XH:** 1A, 1B, 2A, 2C, 3B;
 361 **XL:** 1A, 1B, 2A, 2C, 3A, 3B.

362 **Financial disclosure and conflict of interest statement**

363 This work was supported by the National Institutes of Health (NIH) Pathway to
 364 Independence Award (K99/R00 5R00NS092996-03), the Brain Initiative award
 365 (1RF1MH123247-01), and the NIH R01 award (1R01NS113889-01A1). This work was also
 366 supported by the National Institute of Neurological Disorders and Stroke Parkinson's Disease
 367 Biomarker Program (NS06722 and NS112008 to X.H), the National Institute of Aging
 368 (AG067651 to G.B), the Hershey Medical Center General Clinical Research Center (National
 369 Center for Research Resources, Grant UL1 RR033184 that is now at the National Center for
 370 Advancing Translational Sciences, Grant UL1 TR000127), the PA Department of Health
 371 Tobacco CURE Funds, and the Penn State Translational Brain Research Center. The authors
 372 report no financial interests or potential conflicts of interest.

373

References

1. Parkinson J. An essay on shaking palsy. 1817; **14**: 223- 236.
2. Venda LL, Cragg SJ, Buchman VL, Wade-Martins R. α -Synuclein and dopamine at the crossroads of Parkinson's disease. *Trends Neurosci.* 2010; **33**: 559- 568.
3. Aarsland D, Kurz MW. The epidemiology of dementia associated with Parkinson disease. *J. Neurol. Sci.* 2010; **289**: 18- 22.
4. Mattila PM, Rinne JO, Helenius H, Dickson DW, R  ytt   M. Alpha-synuclein-immunoreactive cortical Lewy bodies are associated with cognitive impairment in Parkinson's disease. *Acta Neuropathol.* 2000; **100**: 285- 290.
5. Hurtig HI, Trojanowski JQ, Galvin J, et al. Alpha-synuclein cortical Lewy bodies correlate with dementia in Parkinson's disease. *Neurology.* 2000; **54**: 1916- 1921.
6. Lei P, Ayton S, Finkelstein DI, et al. Tau protein: Relevance to Parkinson's disease. *Int. J. Biochem. Cell Biol.* 2010; **42**: 1775- 1778.
7. Zhang X, Gao F, Wang D, et al. Tau pathology in Parkinson's disease. *Front. Neurol.* 2018; **9**.
8. Goris A, Williams-Gray CH, Clark GR, et al. Tau and α -synuclein in susceptibility to, and dementia in, Parkinson's disease. *Ann. Neurol.* 2007; **62**: 145- 153.
9. Vermersch P, Delacourte A, Javoy-Agid F, Hauw J-J, Agid Y. Dementia in Parkinson's disease: Biochemical evidence for cortical involvement using the immunodetection of abnormal tau proteins. *Ann. Neurol.* 1993; **33**: 445- 450.
10. Irwin DJ, Grossman M, Weintraub D, et al. Neuropathological and genetic correlates of survival and dementia onset in synucleinopathies: a retrospective analysis. *Lancet Neurol.* 2017; **16**: 55-65.
11. Jessen NA, Munk ASF, Lundgaard I, Nedergaard M. The Glymphatic System: A Beginner's Guide. *Neurochem. Res.* 2015; **40**: 2583- 2599.

12. Sundaram S, Hughes RL, Peterson E, et al. Establishing a framework for neuropathological correlates and glymphatic system functioning in Parkinson's disease. *Neurosci. Biobehav. Rev.* 2019; **103**: 305- 315.
13. Valdinocci D, Radford RAW, Goulding M, et al. Extracellular interactions of Alpha-synuclein in multiple system atrophy. *Int. J. Mol. Sci.* 2018; **19**: 4219.
14. Tarasoff-Conway JM, Carare RO, Osorio RS, et al. Clearance systems in the brain - Implications for Alzheimer disease. *Nat. Rev. Neurol.* 2015; **11**: 457- 470.
15. Holth JK, Fritsch SK, Wang C, et al. The sleep-wake cycle regulates brain interstitial fluid tau in mice and CSF tau in humans. *Science (80-.).* 2019; **363**: 880- 884.
16. Mestre H, Mori Y, Nedergaard M. The Brain's Glymphatic System: Current Controversies. *Trends Neurosci.* 2020; **43**: 458- 466.
17. Musiek ES, Xiong DD, Holtzman DM. Sleep, circadian rhythms, and the pathogenesis of Alzheimer disease. *Exp. Mol. Med.* 2015; **47**: e148.
18. Xie L, Kang H, Xu Q, et al. Sleep drives metabolite clearance from the adult brain. *Science (80-.).* 2013; **342**: 373- 377.
19. Iliff JJ, Wang M, Liao Y, et al. A paravascular pathway facilitates CSF flow through the brain parenchyma and the clearance of interstitial solutes, including amyloid β . *Sci. Transl. Med.* 2012; **4**: 147.
20. Iliff JJ, Lee H, Yu M, et al. Brain-wide pathway for waste clearance captured by contrast-enhanced MRI. *J. Clin. Invest.* 2013; **123**: 1299- 1309.
21. Eide PK, Ringstad G. MRI with intrathecal MRI gadolinium contrast medium administration: a possible method to assess glymphatic function in human brain. *Acta Radiol. Open.* 2015; **4**: 1-5.
22. Ringstad G, Valnes LM, Dale AM, et al. Brain-wide glymphatic enhancement and clearance in

- humans assessed with MRI. *JCI insight*. 2018; **3**: e121537.
23. Taoka T, Masutani Y, Kawai H, et al. Evaluation of glymphatic system activity with the diffusion MR technique: diffusion tensor image analysis along the perivascular space (DTI-ALPS) in Alzheimer's disease cases. *Jpn. J. Radiol.* 2017; **35**: 172- 178.
24. Harrison IF, Siow B, Akilo AB, et al. Non-1 invasive imaging of CSF-mediated brain clearance pathways via assessment of perivascular fluid movement with diffusion tensor MRI. *Elife*. 2018; **7**: e34028.
25. Kiviniemi V, Wang X, Korhonen V, et al. Ultra-fast magnetic resonance encephalography of physiological brain activity-Glymphatic pulsation mechanisms? *J. Cereb. Blood Flow Metab.* 2016; **36**: 1033- 1045.
26. Fukunaga M, Horovitz SG, van Gelderen P, et al. Large-amplitude, spatially correlated fluctuations in BOLD fMRI signals during extended rest and early sleep stages. *Magn. Reson. Imaging*. 2006; **24**: 979- 972.
27. Horovitz SG, Fukunaga M, De Zwart JA, et al. Low frequency BOLD fluctuations during resting wakefulness and light sleep: A simultaneous EEG-fMRI study. *Hum. Brain Mapp*. 2008; **29**: 671- 682.
28. Liu X, De Zwart JA, Schölvinck ML, et al. Subcortical evidence for a contribution of arousal to fMRI studies of brain activity. *Nat. Commun.* 2018; **9**: 395.
29. Özbay PS, Chang C, Picchioni D, et al. Contribution of systemic vascular effects to fMRI activity in white matter. *Neuroimage*. 2018; **176**: 541- 549.
30. Shmueli K, van Gelderen P, de Zwart JA, et al. Low-frequency fluctuations in the cardiac rate as a source of variance in the resting-state fMRI BOLD signal. *Neuroimage*. 2007; **38**: 306- 320.
31. Chang C, Cunningham JP, Glover GH. Influence of heart rate on the BOLD signal: The cardiac

response function. *Neuroimage*. 2009; **44**: 857- 869.

32. Birn RM, Diamond JB, Smith MA, Bandettini PA. Separating respiratory-variation-related fluctuations from neuronal-activity-related fluctuations in fMRI. *Neuroimage*. 2006; **31**: 1536-1548.
33. Power JD, Plitt M, Gotts SJ, et al. Ridding fMRI data of motion-related influences: Removal of signals with distinct spatial and physical bases in multiecho data. *Proc. Natl. Acad. Sci. U. S. A.* 2018; **115**: E2105- E2114.
34. Gu Y, Han F, Sainburg LE, Liu X. Transient Arousal Modulations Contribute to Resting-State Functional Connectivity Changes Associated with Head Motion Parameters. *Cereb. Cortex*. 2020; **30**: 5242- 5256.
35. Tong Y, Yao J (Fiona), Chen JJ, Frederick B de B. The resting-state fMRI arterial signal predicts differential blood transit time through the brain. *J. Cereb. Blood Flow Metab.* 2019; **39**: 1148-1160.
36. Schley D, Carare-Nnadi R, Please CP, Perry VH, Weller RO. Mechanisms to explain the reverse perivascular transport of solutes out of the brain. *J. Theor. Biol.* 2006; **238**: 962- 974.
37. Iliff JJ, Wang M, Zeppenfeld DM, et al. Cerebral arterial pulsation drives paravascular CSF-Interstitial fluid exchange in the murine brain. *J. Neurosci.* 2013; **33**: 18190- 18199.
38. Klose U, Strik C, Kiefer C, Grodd W. Detection of a relation between respiration and CSF pulsation with an echoplanar technique. *J. Magn. Reson. Imaging*. 2000; **11**: 438- 444.
39. Yamada S, Miyazaki M, Yamashita Y, et al. Influence of respiration on cerebrospinal fluid movement using magnetic resonance spin labeling. *Fluids Barriers CNS*. 2013; **10**: 36.
40. Mestre H, Tithof J, Du T, et al. Flow of cerebrospinal fluid is driven by arterial pulsations and is reduced in hypertension. *Nat. Commun.* 2018; **9**: 4878.

41. Fultz NE, Bonmassar G, Setsompop K, et al. Coupled electrophysiological, hemodynamic, and cerebrospinal fluid oscillations in human sleep. *Science* (80-.). 2019; **366**: 628- 631.
42. Stefanis L. α -Synuclein in Parkinson's disease. *Cold Spring Harb. Perspect. Med.* 2012; **2**: a009399.
43. Emmanouilidou E, Elenis D, Papasilekas T, et al. Assessment of α -synuclein secretion in mouse and human brain parenchyma. *PLoS One*. 2011; **6**: e22225.
44. Harrison IF, Ismail O, Machhada A, et al. Impaired glymphatic function and clearance of tau in an Alzheimer's disease model. *Brain*. 2020; **143**: 2576-2 593.
45. Wills J, Jones J, Haggerty T, et al. Elevated tauopathy and alpha-synuclein pathology in postmortem Parkinson's disease brains with and without dementia. *Exp. Neurol.* 2010; **225**: 210-218.
46. Irwin DJ, Lee VMY, Trojanowski JQ. Parkinson's disease dementia: Convergence of α -synuclein, tau and amyloid- β pathologies. *Nat. Rev. Neurosci.* 2013; **14**: 626- 636.
47. Hughes AJ, Daniel SE, Kilford L, Lees AJ. Accuracy of clinical diagnosis of idiopathic Parkinson's disease: A clinico-pathological study of 100 cases. *J. Neurol. Neurosurg. Psychiatry*. 1992; **55**: 181-184.
48. Goetz CG, Fahn S, Martinez-Martin P, et al. Movement disorder society-sponsored revision of the unified Parkinson's disease rating scale (MDS-UPDRS): Process, format, and clinimetric testing plan. *Mov. Disord.* 2007; **22**: 41-47.
49. Lewis MM, Harkins E, Lee EY, et al. Clinical Progression of Parkinson's Disease: Insights from the NINDS Common Data Elements. *J. Parkinsons. Dis.* 2020; **10**: 1075- 1085.
50. Tomlinson CL, Stowe R, Patel S, et al. Systematic review of levodopa dose equivalency reporting in Parkinson's disease. *Mov. Disord.* 2010; **25**: 2649- 2653.

51. Nasreddine ZS, Phillips NA, Bédirian V, et al. The Montreal Cognitive Assessment, MoCA: A brief screening tool for mild cognitive impairment. *J. Am. Geriatr. Soc.* 2005; **53**: 695- 699.
52. Williams JBW. A Structured Interview Guide for the Hamilton Depression Rating Scale. *Arch. Gen. Psychiatry.* 1988; **45**: 742- 747.
53. Dalrymple-Alford JC, MacAskill MR, Nakas CT, et al. The MoCA: Well-suited screen for cognitive impairment in Parkinson disease. *Neurology.* 2010; **75**: 1717- 1725.
54. Biswal BB, Mennes M, Zuo XN, et al. Toward discovery science of human brain function. *Proc. Natl. Acad. Sci. U. S. A.* 2010; **107**: 4734- 4739.
55. Mazziotta JC, Toga AW, Evans A, Fox P, Lancaster J. A probabilistic atlas of the human brain: Theory and rationale for its development. *Neuroimage.* 1995; **2**: 89- 101.
56. Babiloni C, Frisoni GB, Pievani M, et al. Hippocampal volume and cortical sources of EEG alpha rhythms in mild cognitive impairment and Alzheimer disease. *Neuroimage.* 2009; **44**: 123- 135.
57. Velayudhan L, Proitsi P, Westman E, et al. Entorhinal cortex thickness predicts cognitive decline in Alzheimer's disease. *J. Alzheimer's Dis.* 2013; **33**: 755- 766.
58. Fjell AM, Westlye LT, Grydeland H, et al. Accelerating cortical thinning: Unique to dementia or universal in aging? *Cereb. Cortex.* 2014; **24**: 919- 934.
59. Ma X, Li Z, Jing B, et al. Identify the atrophy of Alzheimer's disease, mild cognitive impairment and normal aging using morphometric MRI analysis. *Front. Aging Neurosci.* 2016; **8**: 243.
60. Fischl B. FreeSurfer. *Neuroimage.* 2012; **62**: 774- 781.
61. Hoops S, Nazem S, Siderowf AD, et al. Validity of the MoCA and MMSE in the detection of MCI and dementia in Parkinson disease. *Neurology.* 2009; **75**: 478.
62. Smith SM, Zhang Y, Jenkinson M, et al. Accurate, robust, and automated longitudinal and cross-sectional brain change analysis. *Neuroimage.* 2002; **17**: 479- 489.

63. Aquino KM, Fulcher BD, Parkes L, Sabaroedin K, Fornito A. Identifying and removing widespread signal deflections from fMRI data: Rethinking the global signal regression problem. *Neuroimage*. 2020; **212**: 116614.
64. Desikan RS, Ségonne F, Fischl B, et al. An automated labeling system for subdividing the human cerebral cortex on MRI scans into gyral based regions of interest. *Neuroimage*. 2006; **31**: 968- 980.
65. Gao JH, Liu HL. Inflow effects on functional MRI. *Neuroimage*. 2012; **62**: 1035- 1039.
66. Power JD, Barnes KA, Snyder AZ, Schlaggar BL, Petersen SE. Spurious but systematic correlations in functional connectivity MRI networks arise from subject motion. *Neuroimage*. 2012; **59**: 2142- 2154.
67. Chang C, Leopold DA, Schölvinck ML, et al. Tracking brain arousal fluctuations with fMRI. *Proc. Natl. Acad. Sci. U. S. A.* 2016; **113**: 4518- 4523.
68. Fisher RA. On the Interpretation of χ^2 from Contingency Tables, and the Calculation of P. *J. R. Stat. Soc.* 1922; **85**: 87- 94.
69. Bonferroni CE. 1936 Teoria statistica delle classi e calcolo delle probabilità. *Pubbl. del R Ist. Super. di Sci. Econ. e Commer. di Firenze*. 1936; 1493- 1494.
70. Liu TT, Nalci A, Falahpour M. The global signal in fMRI: Nuisance or Information? *Neuroimage*. 2017; **150**: 213- 229.
71. Yeo BTT, Tandi J, Chee MWL. Functional connectivity during rested wakefulness predicts vulnerability to sleep deprivation. *Neuroimage*. 2015; **111**: 147- 158.
72. Wong CW, Olafsson V, Tal O, Liu TT. The amplitude of the resting-state fMRI global signal is related to EEG vigilance measures. *Neuroimage*. 2013; **83**: 983- 990.
73. Kiviniemi VJ, Haanpää H, Kantola JH, et al. Midazolam sedation increases fluctuation and synchrony of the resting brain BOLD signal. *Magn. Reson. Imaging*. 2005; **23**: 531- 537.

74. van Veluw SJ, Hou SS, Calvo-Rodriguez M, et al. Vasomotion as a Driving Force for Paravascular Clearance in the Awake Mouse Brain. *Neuron*. 2020; **105**: 549- 561.
75. Thompson PM, Hayashi KM, De Zubicaray G, et al. Dynamics of gray matter loss in Alzheimer's disease. *J. Neurosci*. 2003; **23**: 994-1005.
76. Long X, Zhang L, Liao W, Jiang C, Qiu B. Distinct laterality alterations distinguish mild cognitive impairment and Alzheimer's disease from healthy aging: Statistical parametric mapping with high resolution MRI. *Hum. Brain Mapp*. 2013; **34**: 3400- 3410.
77. Hasan KM, Mwangi B, Cao B, et al. Entorhinal Cortex Thickness across the Human Lifespan. *J. Neuroimaging*. 2016; **26**: 278- 282.
78. Braak H, Braak E. The human entorhinal cortex: normal morphology and lamina-specific pathology in various diseases. *Neurosci. Res*. 1992; **15**: 6-31.
79. Braak H, Braak E. Neuropathological staging of Alzheimer-related changes. *Acta Neuropathol*. 1991; **82**: 239- 259.
80. Braak H, Del Tredici K, Rüb U, et al. Staging of brain pathology related to sporadic Parkinson's disease. *Neurobiol. Aging*. 2003; **24**: 197- 211.

Figures

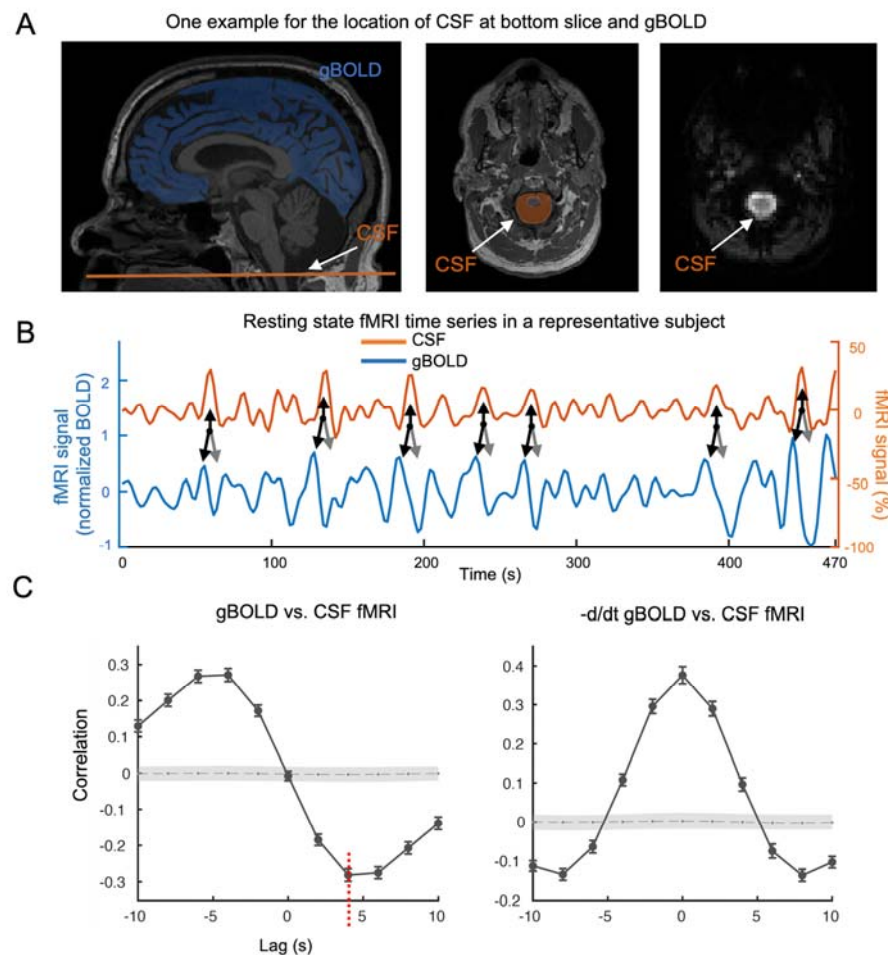


Fig. 1. Systematic coupling between the gBOLD and CSF signals measured by rsfMRI. (A) The gBOLD and CSF fMRI signals were extracted from the whole-brain gray matter regions (the blue mask on a T1-weighted structural MRI in the left panel) and the CSF region at the bottom slice of the fMRI acquisition (the bright region in the right panel and the orange-shaded area in the middle panel), respectively. (B) The gBOLD and CSF signal from a representative subject (control) showed corresponding changes of large amplitude. Large CSF peaks (upwards black arrows) often are preceded by a large positive gBOLD peak (downwards black arrows) and followed by a large negative gBOLD peak (gray arrows). (C) The averaged cross-correlation function (N = 118 subjects) between the gBOLD signal (reference) and the CSF signal (left), as well as between the first-order negative derivative of gBOLD signal (reference) and the CSF signal (right). The gray dashed line and the shaded region mark 95% confidence intervals for the mean correlation computed on shuffled signals (see **Materials and methods** for details). The

565 cross-correlations between the gBOLD and CSF signal at the +4 seconds lag (mean r : -0.28 ; $p <$
 566 0.0001 , permutation test with $N = 10,000$; red dashed line) was used to represent “the gBOLD-
 567 CSF coupling” for subsequent analyses.

568

569

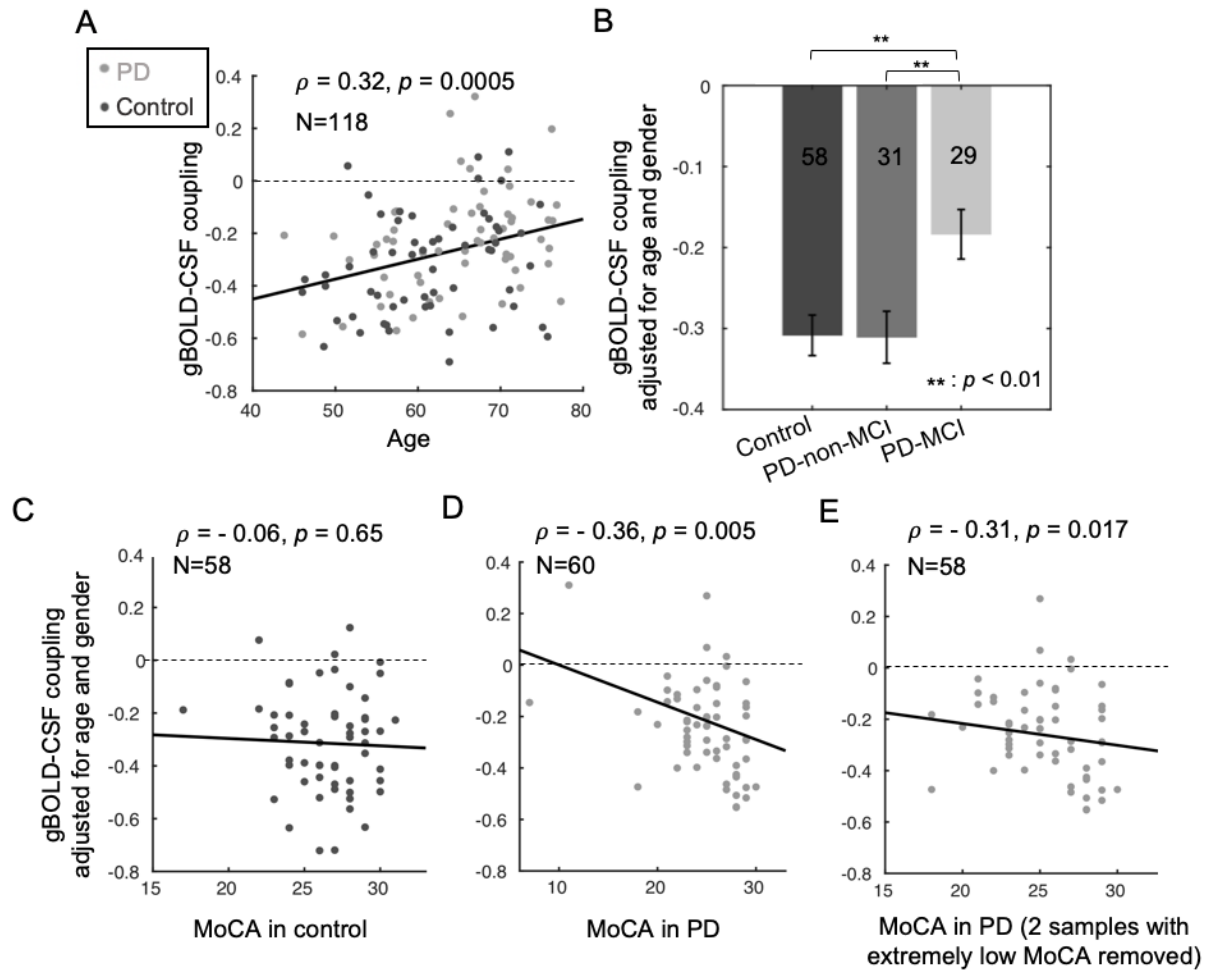


Fig. 2. The associations of gBOLD-CSF coupling to age, disease condition, and MoCA. (A) Older subjects have a weaker (less negative) gBOLD-CSF coupling (Spearman's $\rho = 0.32$, $p = 0.0005$). (B) Compared with controls and PD-non-MCI subjects, PD-MCI subjects have decreased gBOLD-CSF coupling strength (adjusted for age and gender; $p \leq 0.006$, two-sample t-test). (C-D) The correlation between the gBOLD-CSF coupling (adjusted for age and gender) and MoCA scores is significant in the PD group ($\rho = -0.36$, $p = 0.005$, $p_{\text{Bonferroni}} = 0.01$; D) but not in the controls ($\rho = -0.06$, $p = 0.65$; C). (E) The significant correlation between gBOLD-CSF coupling and MoCA within PD subjects remained significant when removing the two subjects with extremely low MoCA scores ($\rho = -0.31$, $p = 0.017$, $p_{\text{Bonferroni}} = 0.034$). The dashed lines indicate where the gBOLD-CSF coupling equals zero.

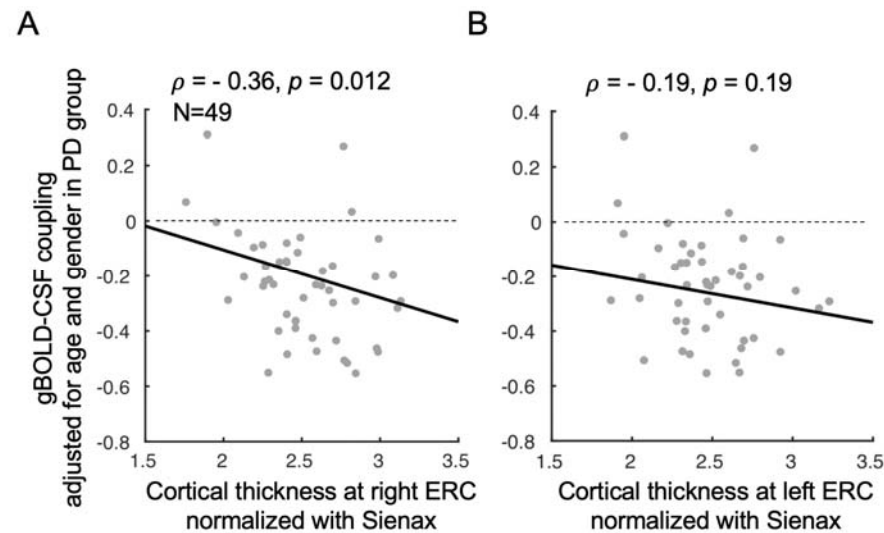


Fig. 3. Associations between gBOLD-CSF coupling and thickness of the entorhinal cortex in PD patients. The PD patients with thinner right ERC tend to have weaker gBOLD-CSF coupling (Spearman's $\rho = -0.36$, $p = 0.012$, $p_{\text{Bonferroni}} = 0.024$) (A). This association is similar but not significant ($\rho = -0.19$, $p = 0.19$, $p_{\text{Bonferroni}} = 0.38$) for the left ERC (B). The ERC thickness was normalized with the SiENx index.⁶²

Table 1: Characteristics of the cohort

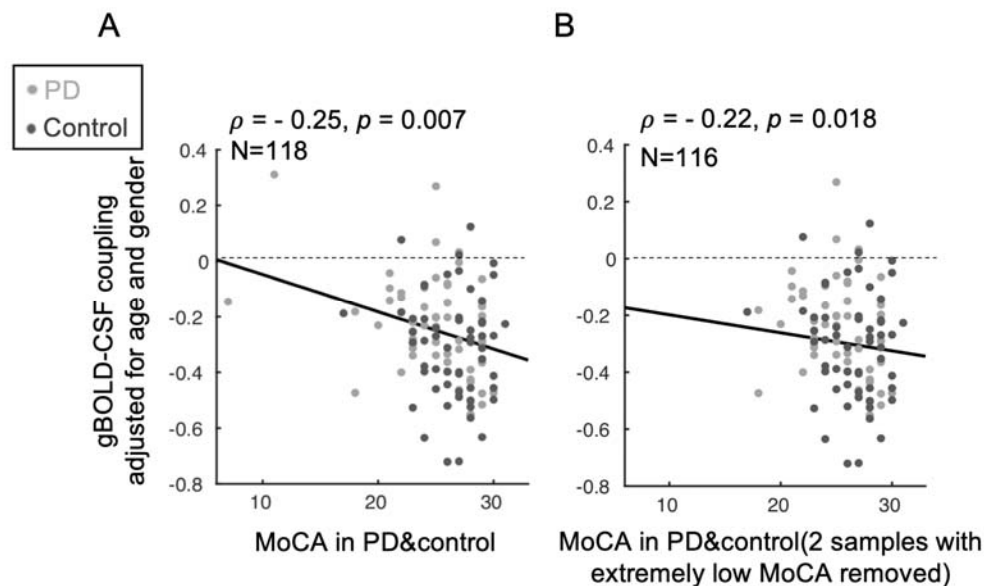
	Controls (N=58)	PD (N=60)	P value
Age, y	61.4 (8.0)	64.7 (8.2)	0.027
Gender (Male/ Female)	31/27	6/24	0.58
Disease duration, y	—	6.6 (5.7)	—
UPDRS-I	—	10.6 (7.9)	—
UPDRS-II	—	9.4 (8.5)	—
UPDRS-III	—	22.2 (20.0)	—
LEDD, mg	—	736 (487)	—
MoCA	26.5 (2.6)	24.8 (4.1)	0.009
HAM-D	4.0 (3.3)	7.8(4.6)	4.3×10^{-5}

Data represent the mean and standard deviation (in parentheses) unless otherwise indicated.

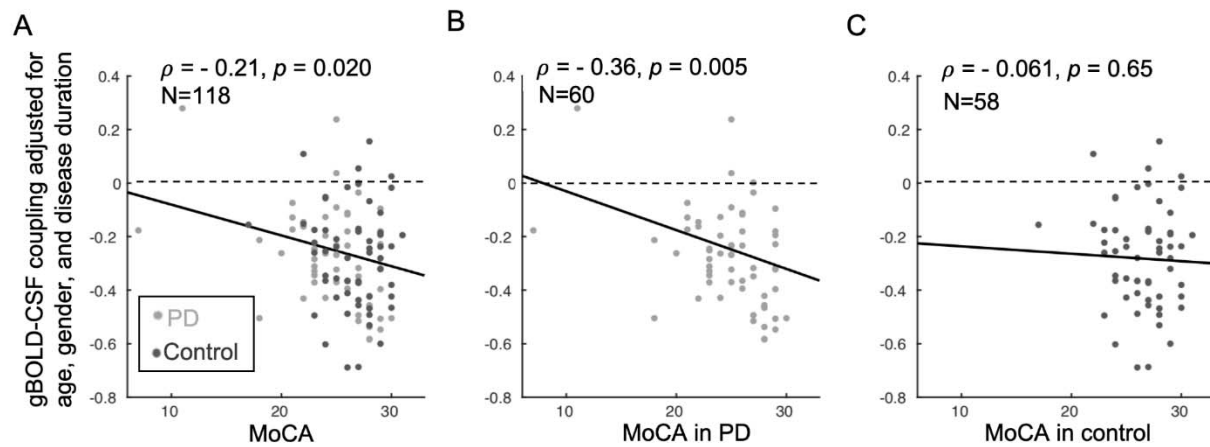
Pairwise comparisons were performed based on the two-sample t-test for all measures except for gender that used the Fisher exact test.

Abbreviation: PD, Parkinson's disease group; UPDRS: Unified Parkinson's Disease Rating Scale; LEDD: levodopa equivalent daily dose; MoCA: Montreal Cognitive Assessment; HAM-D: Hamilton Depression Rating Scale.

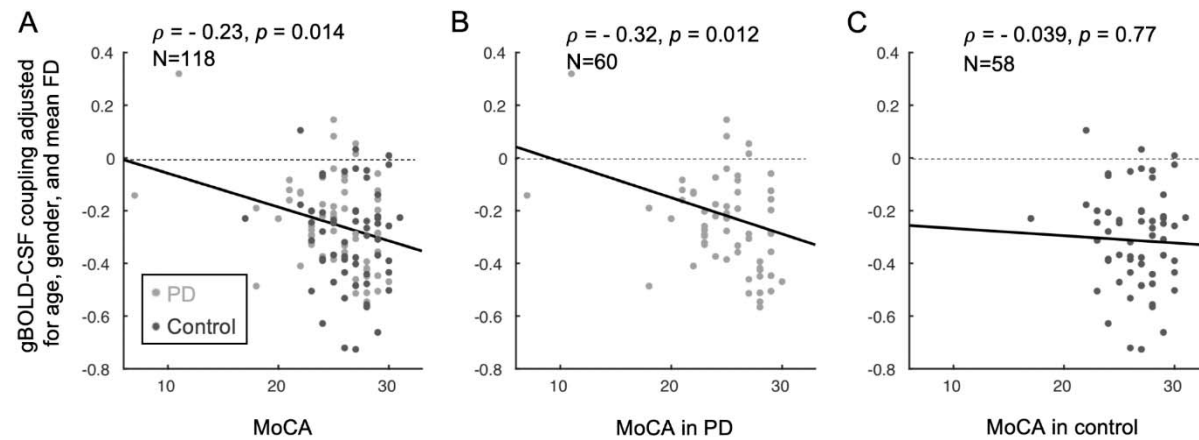
Supplemental files



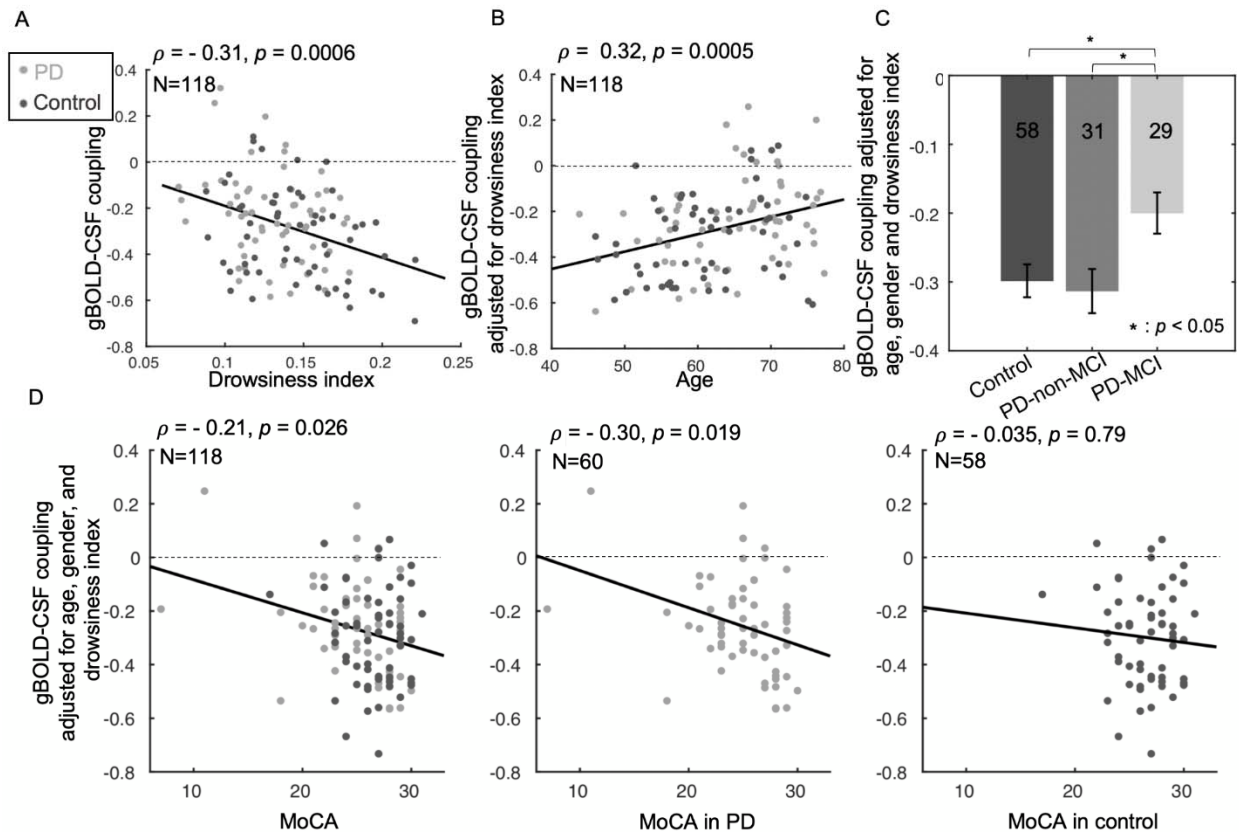
Suppl. Fig. 1. The association between the gBOLD-CSF coupling and MoCA remains significant ($p < 0.018$) in the entire cohort of subjects (A) and after removing two high leverage samples (from two PD subjects) with extremely low MoCA scores (B).



Suppl. Fig. 2. The associations between the gBOLD-CSF coupling and MoCA remains significant ($p < 0.05$) for both the entire group of subjects (A) and the PD group (B), after controlling the age, gender, and disease duration, while this significant correlation cannot be found in controls (C).



Suppl. Fig. 3. The association between the gBOLD-CSF coupling and MoCA remains significant ($p < 0.05$, corrected) for both the overall group of subjects (A) and within Parkinson's subjects (B), after controlling the age, gender, and head motion, whereas the correlation was absent in controls (C).



Suppl. Fig. 4. The association between the sleep-dependent gBOLD-CSF coupling and age,

group, and MoCA scores is not driven by changes in the drowsiness index. (A) The gBOLD-

CSF coupling was correlated significantly with the drowsiness index (increased drowsiness

index corresponds to a drowsier state) in all subjects, which is quantified based on the similarity

between the rsfMRI time-series and a drowsiness template. (B) When adjusted for the

drowsiness index, weaker gBOLD-CSF coupling strength remained significantly associated with

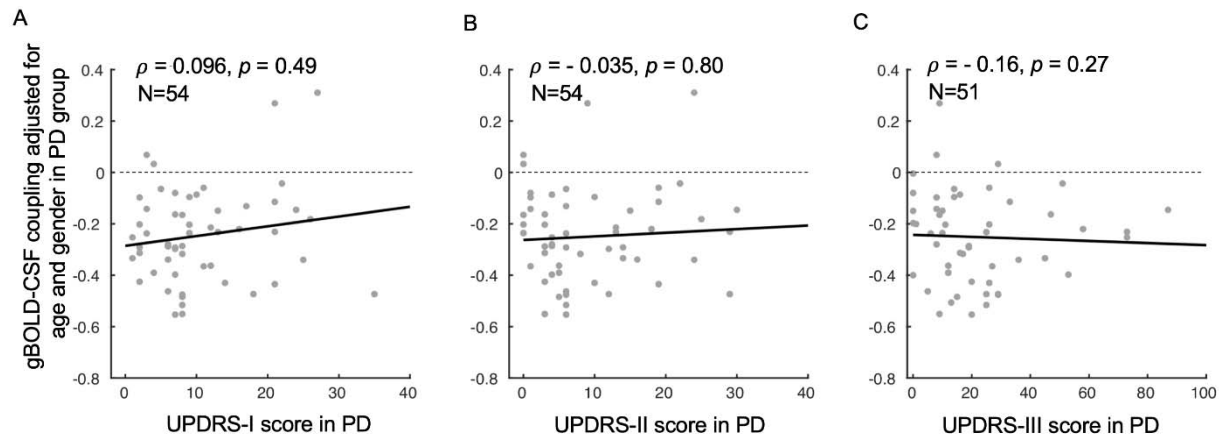
increasing age ($\rho = 0.32, p < 0.001$). (C) PD-MCI subjects had decreased gBOLD-CSF coupling

compared to control or PD-non-MCI after adjusting for the drowsiness index (both $p \leq 0.014$).

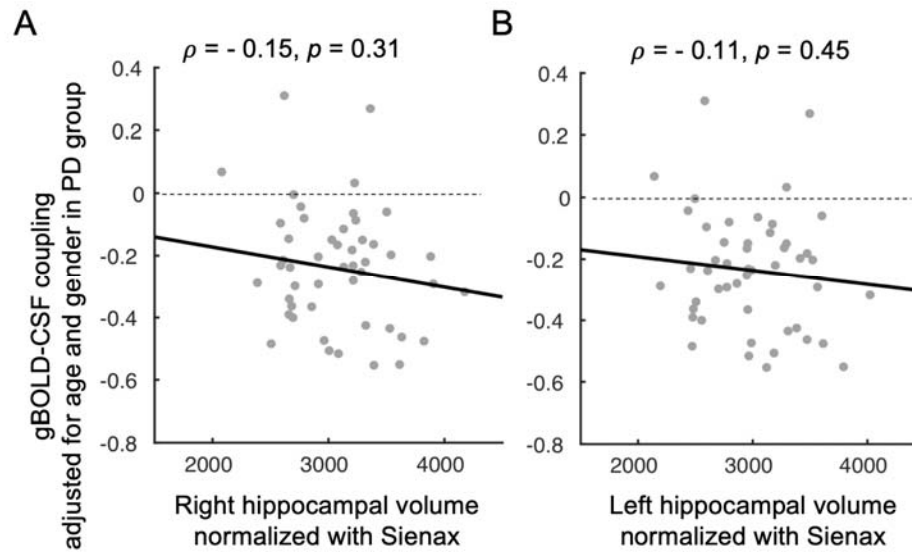
(D) Similar to Fig. 2C, gBOLD-CSF coupling (age, gender, and drowsiness index adjusted)

remained significantly correlated with MoCA scores across both the entire group of subjects and

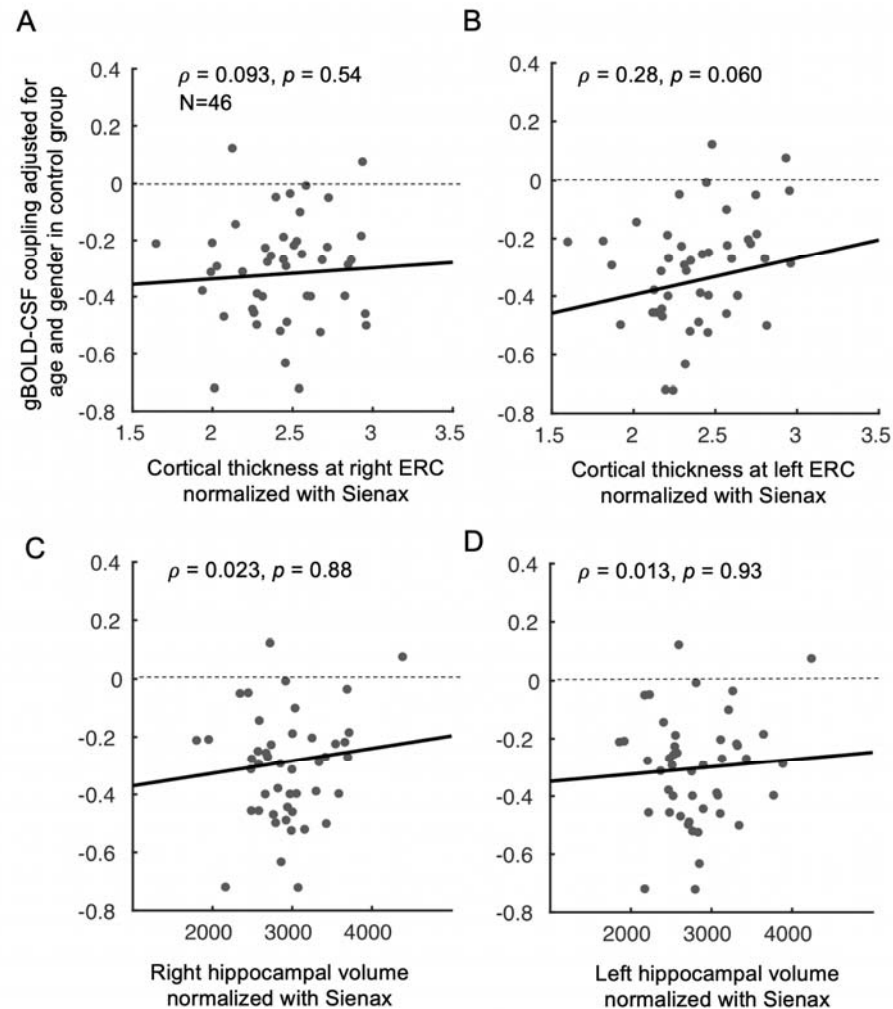
628 within Parkinson's but not for controls. The dashed lines indicate where the gBOLD-CSF
629 coupling equals zero.



Suppl. Fig. 5. The associations (linear regression) between the gBOLD-CSF coupling (adjusted for age and gender) and MDS-UPDRS scores were not significant ($p > 0.05$) within Parkinson's subjects. The linear regression lines were estimated based on least-squares fitting.



Suppl. Fig. S6. Associations between gBOLD-CSF coupling and structural measures of the hippocampus in PD patients. (A-B) The gBOLD-CSF coupling showed a negative correlation with the bilateral hippocampal volumes (normalized with the SiENx index),⁶² but none of the correlations were statistically significant ($p > 0.05$).



Suppl. Fig. S7. gBOLD-CSF coupling and structural measures in the entorhinal cortex and hippocampus were not correlated in controls (all $p > 0.05$). The linear regression lines were estimated based on least-squares fitting.